Structure of double Keggin-Ti/W-mixed polyanion [(A-β-GeTi$_3$W$_9$O$_{37}$)$_2$O$_3$]$^{14-}$ and multielectron-transfer-based photocatalyic H$_2$-generation

Toshihiro Yamase [a,b,*], Xiaoou Cao [a,b], Satomi Yazaki [a,b]

[a] *Chemical Resources Laboratory, Tokyo Institute of Technology, R1-21, 4259 Nagatsuta, Midori-ku, Yokohama 226-8503, Japan*
[b] *Creation of Bio-devices and Bio-systems with Chemical and Biological Molecules for Medical Use, CREST,*
Japan Science and Technology Agency (JST), Japan

Available online 24 August 2006

Abstract

[(A-β-GeW$_9$Ti$_3$O$_{37}$)$_2$O$_3$]$^{14-}$ (**1a**) is isolated as K$^+$/Na$^+$/H$^+$ salt, K$_9$NaH$_4$[(β-GeW$_9$Ti$_3$O$_{37}$)$_2$O$_3$]·40.5H$_2$O (**1**), and characterized by single-crystal X-ray structural and ^{183}W NMR spectral analyses in comparison with [(A-α-GeW$_9$Ti$_3$O$_{37}$)$_2$O$_3$]$^{14-}$ (**2a**) previously isolated as K$_9$H$_5$[(α-GeW$_9$Ti$_3$O$_{37}$)$_2$O$_3$]·16H$_2$O (**2**). Two isomers of **1a** and **2a** have local symmetry of D_{3h} and are stable in aqueous solutions at least at pH values of ≤7. The photocatalytic H$_2$-formation for the dehydrogenative oxidation of methanol (CH$_3$OH → H$_2$ + HCHO) with **1** and **2** is investigated with a help of electronic and ESR spectra and electrochemistry, and is explained in terms of the two-electron reduction of protons at the central Ti^{III}–O–Ti^{III} linkage of the corner-shared TiO$_6$ octahedra connecting two half molecules.
© 2006 Elsevier B.V. All rights reserved.

Keywords: Double Keggin-Ti/W-mixed polyanions; Photocatalysis; ^{183}W NMR spectroscopy; H$_2$ generation; Multielectron redox reaction

1. Introduction

Ti-substituted Keggin polyoxotungstates such as [PTiW$_{11}$O$_{40}$]$^{5-}$, [PTi$_2$W$_{10}$O$_{40}$]$^{7-}$, and [PTi$_2$W$_{10}$O$_{38}$(O$_2$)$_2$]$^{7-}$ work as not only an oxidation catalyst for the epoxidation of alkenes with H$_2$O$_2$ [1–4] but also a photocatalyst for the dehydrogenative oxidation of organic substrates with an accompanying H$_2$-formation [5,6]. In the course of our paying a special attention to the chemical structure of the Ti site in the polyanions as a net catalyst for these reactions, multi-electron oxidation and reduction species at the Ti sites two-electron oxidation hydroperoxotitanium site Ti^{IV}(OOH) and its two-electron oxidation species Ti^{IV}(OOH)$_2$, and four-electron reduction site ⌐Ti^{III}-O-W^V-O-Ti^{III}-O-W^V-O⌐ (for the reduction of CO$_2$) have been proposed. However, molecular aspect of a net catalyst for such reactions remains still unclear and is sometimes with a matter of controversy, especially for the monophasic H$_2$O$_2$-epoxidation [3,4]. An understanding about multielectron redox reactions (usually involving proton transfer) has yet to be real-

ized. With a use of K$_9$NaH$_4$[(β-GeW$_9$Ti$_3$O$_{37}$)$_2$O$_3$]·40.5H$_2$O (**1**) and K$_9$H$_5$[(α-GeW$_9$Ti$_3$O$_{37}$)$_2$O$_3$]·16H$_2$O (**2**) we describe here the photocatalytic oxidation of methanol (MeOH) to formaldehyde (HCHO) with an accompanying formation of hydrogen gas (H$_2$) as a simple model of the multi(two)-electron redox reaction for investigation of the molecular structure of a net catalyst.

The anions of the compounds **1** and **2** were D_{3h}-symmetric double Keggin-Ti/W-mixed species [(A-β-GeW$_9$Ti$_3$O$_{37}$)$_2$O$_3$]$^{14-}$ (**1a**) and [(A-α-GeW$_9$Ti$_3$O$_{37}$)$_2$O$_3$]$^{14-}$ (**2a**), respectively. Compound **2** has been X-ray crystallographically characterized and its ^{183}W NMR spectrum in aqueous solution gave two clean peaks with relative intensity of 2:1 and $^2J_{W-O-W}$ of 17.4 Hz [7]. The peak pattern showed that 2 × 6 belt W (W$_{belt}$) atoms appeared downfield of 2 × 3 cap W (W$_{cap}$) atoms, and was different from other double Keggin-structural polyanion derivatives of [(A-β-SiTi$_3$W$_9$O$_{37}$)$_2$O$_3$]$^{14-}$ [8] and [(A-α-SiNb$_3$W$_9$O$_{37}$)$_2$O$_3$]$^{8-}$ [9] which showed that the 2 × 3 W$_{cap}$ atoms appeared downfield of the 2 × 6 W$_{belt}$ atoms with 1:2 relative intensity pattern. Although the ^{183}W NMR spectrum pattern of [(A-α-PTi$_3$W$_9$O$_{37}$)$_2$O$_3$]$^{12-}$ was similar to that of **2a** [10], the ^{183}W NMR spectrum of **1a** has been strongly required for a better understanding of the ^{183}W NMR lines of

* Corresponding author. Tel.: +81 45 924 5260; fax: +81 45 924 5260.
E-mail address: tyamase@res.titech.ac.jp (T. Yamase).

the double Keggin-structural polyanions in conjunction with the stability against the hydrolysis in aqueous solutions [11]. In this paper we discuss both the ^{183}W NMR spectrum and the crystal structure of **1** in comparison with those of **2**, and also show the multi(two)-electron H_2-generation at the corner-shared Ti^{III}–O–Ti^{III} linkages (with 3d^1-electron localized at each TiO_6 site) formed as a result of a single-electron reaction in each of two half molecules.

2. Experimental

2.1. Materials and procedures

$Na_{8.5}H_{1.5}[GeW_9O_{34}]\cdot20H_2O$ [12] and $K_9H_5[(\alpha\text{-}GeW_9Ti_3O_{38.5})_2]\cdot16H_2O$ [7] were prepared and purified according to our published procedures. Each sample was identified in the solid state by comparison of the IR spectrum with that previously reported for the anion. All other chemicals were of Tokyo Kasei G.R. grade and used without further purifications. UV-photolysis of aqueous solutions containing polyanions and MeOH was done in Pyrex tube by using white light from a 500 W super-high pressure mercury/xenon lamp. Measurements of quantum yields of the photoproducts were done for 313 nm light, the chemical actinometry of which was carried out using the potassium ferrioxalate system. Gas chromatography (GC 323) on a Carbosieve S column was employed for analysis of H_2. HCHO in photolytes was determined by means of the acetylacetone procedure [13]. The evacuation to 10^{-4} Torr of solutions for measurement of absorption spectra was done by freeze–pump–thaw cycles. Solutions for electrochemical measurements were flushed with nitrogen gas to exclude oxygen. Contents of K, Ge, Ti, and W were analyzed on a X-ray fluorescence spectrometer (JEOL, JSX-3200). Thermo gravimetric analysis (TGA) was performed on a ULVAC-TGD 9600 /MTS 9000 instrument. IR and UV–vis spectra were recorded on Jasco FT/IR-410 and Jasco V-570 UV–vis–NIR spectrometers, respectively. ^{183}W NMR spectra of **1** or **2** (5×10^{-2} M in D_2O) were obtained on a JEOL JNM-AL300 spectrometer (^{183}W, 12.5 MHz) at 323 K in 10 mm diameter NMR tubes by using 90° pulse, scan repetition time of 15 s, 10,000 scans, and line-broadening factor of 1.0 Hz before FT treatment. Polarograms were recorded on PAR-303A SMDE and -394 instruments and a standard cell with an Ag/AgCl reference electrode. Cyclic voltammograms were measured on Hokuto Denko HZ-3000 HAG-5001 instruments using a glassy carbon (diameter 1.0 mm) working electrode, a Pt-wire counter electrode, and a saturated Ag/AgCl reference electrode. X-band ESR measurements were carried out on a JEOL ESR spectrometer (JES-RE1X).

2.2. Synthesis of $K_9NaH_4[(\beta\text{-}GeW_9Ti_3O_{37})_2O_3]\cdot40.5H_2O$ (**1**)

A 30 g (0.01 mol) of $Na_{8.5}H_{1.5}[GeW_9O_{34}]\cdot20H_2O$ was dissolved in 150 ml H_2O and stirred for 1 h. A 3 ml of $TiCl_4$ was added 10 min dropwise into a resultant suspension with vigorous agitation. The solution at pH $\approx$ 0.5 was stirred for 1 h at room temperature and refluxed for 30 min. A resul-

tant yellowish solution was cooled down to room temperature and filtered. The crude product was precipitated by addition of excess amount of KCl (15 g) to the filtrate. Solid sample was collected on a glass frit and recrystallized in hot water. Slow evaporation of the solution at room temperature for 2–3 weeks yields 6.3 g (yield 20.9%) of colorless thin-plate crystals of $K_9NaH_4[(\beta\text{-}GeW_9Ti_3O_{37})_2O_3]\cdot41.5H_2O$. Anal. Calcd. for $K_9NaH_4[(\beta\text{-}GeW_9Ti_3O_{37})_2O_3]\cdot40.5H_2O$: Ge, 2.39; W, 54.41; Ti, 4.73; K, 5.79; Na, 0.38; H, 1.41. Found: Ge, 2.2; W, 54.1; Ti, 4.8; K, 5.5; Na, 0.2; H, 1.4 %. The water content (40.5 waters of hydration) was determined by thermogravimetric analysis: a weight loss of 12% was observed after heating at 500 °C for 4 h. FT-IR (cm^{-1}, KBr): 962 (m), 879 (w), 819 (s), 765 (vs), 721 (m), 530 (m), 457 (m). ^{183}W NMR (0.05 M in D_2O, pD = 1.0, ref. 2.0 M Na_2WO_4): δ −116.2 (6W, $\Delta\nu_{1/2} = 1.7 \pm 0.1$ Hz), −121.4 ppm (12 W, $\Delta\nu_{1/2} = 1.8 \pm 0.1$ Hz); $^2J_{W-O-W} = 15.9$ Hz.

2.3. Synthesis of $K_9H_5[(\alpha\text{-}GeW_9Ti_3O_{37})_2O_3]\cdot16H_2O$ **2**

2 was prepared according to the method described in the literature [7] and characterized with elemental analysis, and IR and ^{183}W NMR spectra. To suspension of 45 g of $Na_{8.5}H_{1.5}[GeW_9O_{34}]\cdot20H_2O$ in 150 ml of H_2O, 4 ml of $TiCl_4$ was added dropwise with vigorous agitation. The solution (at pH level less than 1.0) was refluxed for 30 min, cooled to room temperature, and filtrated to exclude white precipitates. Thereafter, 15 g of KCl was added to the filtrate, and the crude product as K^+ salt was twice recrystallized; 4.0 g of colorless needle crystals of **2** were obtained. Anal. Calcd. for $K_9H_5[(\alpha\text{-}GeW_9Ti_3O_{37})_2O_3]\cdot16H_2O$: Ge, 2.59; W, 58.90; Ti, 5.11; K, 6.26; H, 0.66. Found: Ge, 2.4; W, 57.8; Ti, 4.8; K, 6.7; H, 0.9. The water content (16 waters of hydration) was determined by thermogravimetric analysis: a weight loss of 5.13% was observed after heating at 500 °C for 4 h. IR (cm^{-1}, KBr): 956 (m), 893 (s), 817 (m), 773 (m), 724 (m), 530 (m), 496 (m), 466 (m). ^{183}W NMR (0.05 M in D_2O, pD = 1.0, ref. 2.0 M Na_2WO_4): δ −107.2 (12 W, $\Delta\nu_{1/2} = 1.5 \pm 0.1$ Hz), −126.4 ppm (6 W, $\Delta\nu_{1/2} = 1.6 \pm 0.1$ Hz); $^2J_{W-O-W} = 17.4$ Hz.

2.4. X-ray crystallography of **1**

X-ray diffraction measurement was made on a Rigaku RAXIS-RAPID Imaging Plate X-ray diffractometer with graphite-monochromated Mo K$_\alpha$ radiation (50 kV, 36 mA, $\lambda = 0.71075$ Å). A colorless thin-platelet crystal of **1** with a size of 0.15 mm × 0.15 mm × 0.05 mm was mounted in a loop in the diffractometer. The reflection intensities were collected at 173 K using an ω-oscillation method with an oscillation width of 3° and an exposure time of 180 s per frame. A 13,674 of the 557,688 collected reflections were unique ($R_{int} = 0.079$), and the equivalent reflections were merged. The unit-cell parameters were determined using 244 reflections with a 2θ range of 0–55.0°. An empirical absorption correction was made with transmission factors ranging from 0.08 to 1.00. The data were corrected for Lorentz and polarization effects. The structure was solved by direct methods (SIR92) and refined on F^2 with all the 4464 observed reflec-
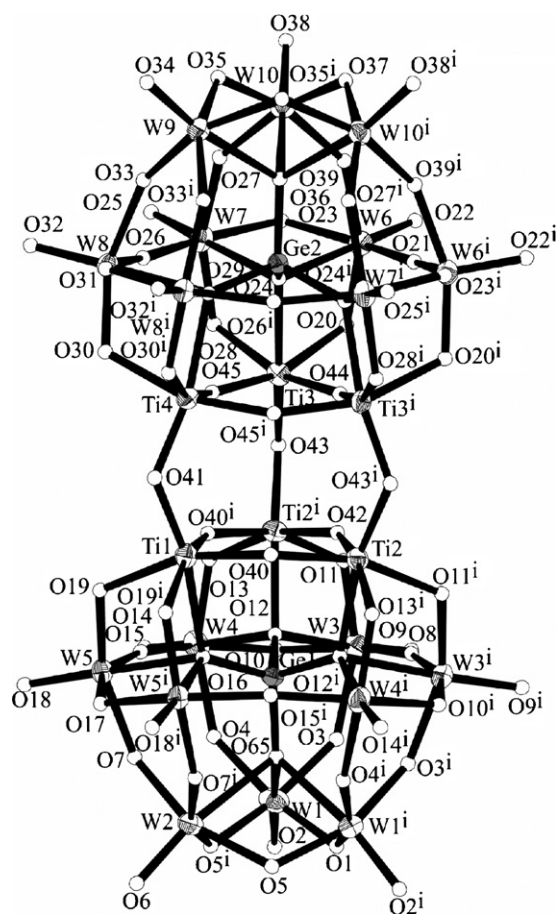
Fig. 1. Structure of $[(A\text{-}\beta\text{-}GeTi_3W_9O_{37})_2O_3]^{14-}$ (**1a**).

tions and 412 variables. Residual difference Fourier peaks with $\Delta\rho_{max} = 3.78\,e\,\text{Å}^{-3}$ and $\Delta\rho_{min} = -3.80\,e\,\text{Å}^{-3}$ were observed at positions 0.10 and 0.08 Å from K3 and W2, respectively. This is due to a large displacement of K3 and W2 atoms, compared with other atoms. Oxygen atoms were refined isotropically, and the other non-hydrogen atoms anisotropically. All calculations were performed using the Crystal-Structure crystallographic software package. Crystal data for $W_{18}Ge_2K_9NaTi_6O_{117.5}H_{85}$ (**1**), $M = 6082.36$, orthorhombic, space group *Pbcm* (No. 57), $a = 13.15(1)$ Å, $b = 38.64(5)$ Å, $c = 21.66(3)$ Å, $V = 11004(23)$ Å^3, $Z = 4$, $D_c = 3.671\,\text{g cm}^{-3}$, $\mu(\text{Mo } K_\alpha) = 201.65\,\text{cm}^{-1}$, final $R_1 = 0.042$ with $I > 2\sigma(I)$, $R_w = 0.077$ with $I > 1\sigma(I)$, and GOF = 1.00.

3. Results and discussion

3.1. Structural characterization of **1** in comparison with **2**

Fig. 1 shows the structure of anion (**1a**) of the compound, $K_9NaH_4[(\beta\text{-}GeW_9Ti_3O_{37})_2O_3]\cdot41.5H_2O$ (**1**), which is so far strongly required to be characterized from a standpoint of the ^{183}W NMR chemical-shift feature of **2a** [8,11]. **1a** comprises two Keggin-structural $[GeTi_3W_9O_{40}]^{10-}$ moieties fused together at three terminal O atoms of the TiO$_6$ octahedra.

Each $[GeTi_3W_9O_{40}]^{10-}$ moiety has an A-β-Ti$_3$W$_9$ configuration with C_{3v} symmetry in which the three TiO$_6$ octahedra are linked to one another by corner-sharing. The double Keggin-Ti/W-mixed polyanion $[(A\text{-}\beta\text{-}GeTi_3W_9O_{37})_2O_3]^{14-}$, has D_{3h} symmetry. Based on this symmetry, the 18 W atoms could be classified into two categories: 6 cap W atoms (W1, W1′, W2, W9, W10, W10′) at the two ends of the anion and 12 belt W atoms between the cap W atoms and the Ti atoms (W3 through W8 and W3′ through W8′). Subsequent to our report of $[(A\text{-}\alpha\text{-}GeTi_3W_9O_{37})_2O_3]^{14-}$ [7] and Finke's report of $[(A\text{-}\beta\text{-}SiTi_3W_9O_{37})_2O_3]^{14-}$ [8] in 1993, several other double Keggin-structural polyanions have been X-ray crystallographically characterized for $[(A\text{-}\alpha\text{-}SiNb_3W_9O_{37})_2O_3]^{8-}$ [9], $[(A\text{-}\alpha\text{-}PTi_3W_9O_{37})_2O_3]^{12-}$ [10], and $[(A\text{-}\alpha\text{-}SiCr_3W_9O_{37})_2O_3]^{20-}$ [14].

The metal–metal distances in the anion are listed in Table S1. The edge-shared Ti···W distances for **1** and **2** are 3.301(8) and 3.282(12) Å, while the edge-shared W···W distances are 3.367(3) and 3.365(5) Å among the cap W atoms, and 3.336(2) and 3.341(7) Å among the belt W atoms, respectively. As was discussed regarding the structure of the $[PTi_2W_{10}O_{40}]^{7-}$ anion, the short Ti···W distances are due to the small electrostatic repulsion between the Ti and W atoms, compared with that between two W atoms [15]. The corner-shared W···W distances for **1** and **2** are 3.700(3) and 3.739(6) Å for the W_{cap}–W_{belt} pairs, 3.786(3) and 3.762(8) Å for the W_{belt}–W_{belt} pairs, respectively. The corner-shared Ti···Ti distances for **1** and **2** are 3.612(10) and 3.64(3) Å within the half molecule and 3.353(10) and 3.362(9) Å at the linkage of the two half-molecules, respectively, which are also shorter than that for the corner-shared W···W pairs. The metal–oxygen bond distances are listed in Table S2. The terminal W–O distances for **1** and **2** are 1.70(3) and 1.75(4) Å at the cap W atoms and 1.70(2) and 1.69(3) Å at the belt ones, respectively. The edge-shared W–O(–Ti) distances for **1** and **2** are 1.87(2) and 1.84(3) Å, respectively, which is significantly shorter than the edge-shared W–O(–W) distances of 1.93(2) and 1.93(5) Å at the cap–cap pairs, 1.96(2) and 1.92(5) Å at the belt–belt pairs, respectively. This is explained by the fact that the O atoms between the Ti and W atoms are attracted toward a more positive W center from a less-positive Ti center. As a result of its *trans* influence, the corner-shared W_{belt}–O(–W_{cap}) distances for **1** and **2** become as long as 2.00(2) and 1.97(3) Å, respectively. Also, the W–O distances of their *trans* position become as short as 1.87(2) and 1.89(3) Å, respectively. The Ti–O distances at the O atoms bridging the two $[GeTi_3W_9O_{40}]^{10-}$ moieties for **1** and **2** are 1.84(3) and 1.82(2) Å, respectively, which are regarded as being single bonds. These O atoms are the terminal O atoms at the three Ti atoms in the hypothetical monomer of $[GeTi_3W_9O_{40}]^{10-}$. In the $[PTi_2W_{10}O_{40}]^{7-}$ anion, the terminal Ti–O bond distances were 1.75–1.77 Å, and the terminal O atoms are expected to be protonated [15,16]. Since the terminal O atoms at the Ti atoms of $[GeTi_3W_9O_{40}]^{10-}$ would be similarly protonated, its dimeric condensation may be possible as follows:
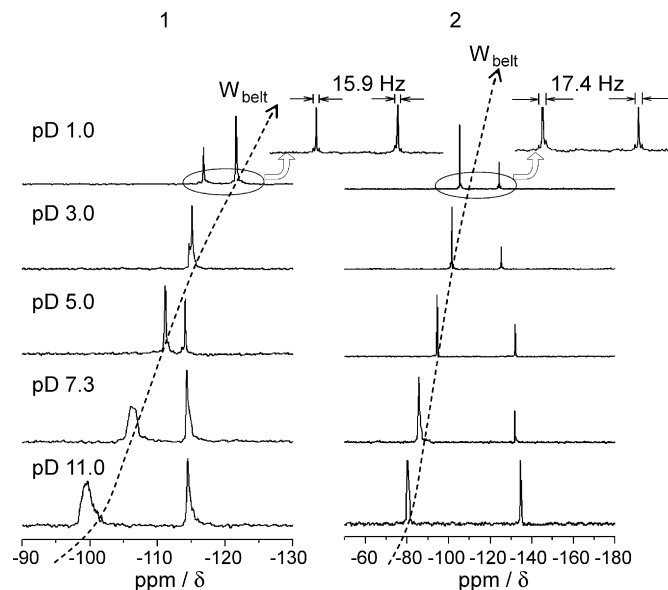
$$[GeTi_3W_9O_{40}]^{10-} + 3H^+ \leftrightarrow [GeTi(OH)_3W_9O_{37}]^{7-}$$
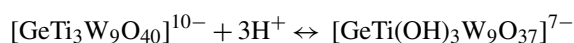
Fig. 2. ^{183}W NMR spectra of $K_9NaH_4[(\beta\text{-}GeW_9Ti_3O_{37})_2O_3]\cdot40.5H_2O$ (**1**) and $K_9H_5[(\alpha\text{-}GeW_9Ti_3O_{37})_2O_3]\cdot16H_2O$ (**2**) on a variety of solution pD levels (1–11).

and

$$2[GeTi(OH)_3W_9O_{37}]^{7-} \leftrightarrow [(GeTi_3W_9O_{37})_2O_3]^{14-} + 3H_2O$$

This indicates that the substitution of W atoms of the Keggin (or other) polyanions for the less-positive heteroatoms gives rise to more negative charge on the polyanion surface, with a resultant easiness for undergoing protonation at the heteroatom sites. Thus, the dimerization induced by a partial replacement of W atoms with less-positive heteroatoms suggests the possibility of a higher degree of oligomerization, as were exemplified by $[(A\text{-}\alpha\text{-}GeTi_3W_9O_{37})_4O_6]^{28-}$ [17]. Table S3 lists the selected bond angles for **1** and **2**. As shown in Tables S1–S3, there are no large differences in the molecular structures of **1a** and **2b**. The most notable change in structure between the two isomers is observed for both the W–O–W bond angles of the corner-shared W_{belt}–W_{cap} atoms (143–147°, average 146° for **1** and 147–156°, average 152° for **2**) and the Ti–O–Ti bond angles of the central corner-shared TiO_6 octahedra connecting two half-molecules (131° for **1** and 135° for **2**). Larger bond angles for these corner-shared WO_6 and TiO_6 octahedra for **2** indicate a stronger bonding of the W–O–W and Ti–O–Ti linkages, compared with **1** [18].

3.2. ^{183}W NMR spectroscopy of **1** in comparison with **2**

Fig. 2 shows the ^{183}W NMR spectra of **1** and **2** on a variety of solution pD levels (1–11). Two ^{183}W NMR lines of W_{belt} and W_{cap} atoms, especially the former lines are shifted with a variation of solution pD levels with little change in the ratio (approximately 2:1) of two line intensities. ^{183}W NMR spectrum of **1a** at pD 1 showed 1:2 intensity lines at −116 and −121 ppm in contrast to the one of **2** with 2:1 lines at −107 and −126 ppm. The $^2J_{W-O-W}$ coupling constants observable for **1** and **2** at pD 1 are about 15.9 and 17.4 Hz at both lines, respectively. A smaller

interaction for **1** is associated with a weaker interaction between the corner-shared W_{cap}–W_{belt} atoms as indicated by a smaller bond angle, compared with **2** (Table S3) [18]: W–O–W bond angles of the corner-shared W_{cap}–W_{belt} atoms for **1** and **2** are 146° and 152°, respectively. This implies a larger extent of localization of negative charges over 2 × 6 W_{belt} atoms for **1** with a resultant shift of the ^{183}W NMR line of the W_{belt} atoms toward up-field due to a larger basicity of the W_{belt} atoms (relative to the W_{cap} atoms) on the replacement of W atoms with less positive Ti atoms in the center of molecule. On the other hand, the electrostatic negativity over the W_{cap} atoms which would be effected by the electronic interaction with the W_{belt} atoms through the corner-shared W_{cap}–O–W_{belt} bonds, would be larger for **2** than for **1**, to result in more up-field shift of the ^{83}W NMR line of the W_{cap} atoms for **2**, as shown in Fig. 2. The chemical formula ($K_9NaH_4[(\beta\text{-}GeW_9Ti_3O_{37})_2O_3]\cdot40.5H_2O$) of **1** (or $K_9H_5[(\alpha\text{-}GeW_9Ti_3O_{37})_2O_3]\cdot16H_2O$ of **2**) strongly suggest the disordered protonation at the 2 × 6 W_{belt} sites. The increasing deprotonation at higher pD levels will results in the down-field shift of the ^{183}W NMR line of the W_{belt} atoms due to an increase of the polarizability (or a decrease of the basicity) of the W_{belt} atoms by the electronic communication with the W_{cap} atoms through the corner-shared W_{belt}–O–W_{cap} bonds. Thus, a change to nearly equal basicity of the two type atoms of W_{belt} and W_{cap} for **1** leads to a coalescence of their ^{183}W NMR lines as shown around at pD 3 (Fig. 2). Interestingly, the ^{183}W NMR lines for **1** and **2** are reversible for a change in the solution pD levels: ^{183}W NMR spectrum of **1** at pD 7.3 showing 2:1 intensity lines at −106 and −114 ppm was changed to the spectrum showing 1:2 intensity lines at −113 and −118 ppm on the acidification to pD 1.1. Also, the crystallographic parameters of the single crystal isolated at pH 7.3 for **1** were the same as at pH 1.1. The situation is the same as for **2**. These behaviors on the variation of solution pH(D) levels for **1** and **2** provide a strong indication of little hydrolysis of **1** (or **2**) at the pH range 1–11, which are quite different from the case of $[(A\text{-}\alpha\text{-}SiNb_3W_9O_{37})_2O_3]^{8-}$ which showed five (with 2:2:2:1:2 line intensities) ^{183}W NMR lines due to the hydrolysis involving a stepwise splitting of the central Nb–O–Nb linkages [19]. No indication of the hydrolysis for **1** (or **2**) may be explained by high degree of the protonation on the $W_{belt}O_6$ octahedral O atoms by the replacement with the tetravalent Ti atoms, compared with the pentavalent Nb atoms for $[(A\text{-}\alpha\text{-}SiNb_3W_9O_{37})_2O_3]^{8-}$.

3.3. Photoinduced blue-coloration and H_2-formation, coupled with HCHO-formation

Fig. 3 shows the electronic absorption spectral changes during the steady-state photolysis of deaerated aqueous solutions containing 0.72 mM (**1**) or (**2**) and 2.5 M MeOH at pH levels of 1.0, 4.5, and 10.3. Fig. 3, inset, shows the UV spectrum of the aqueous solutions containing 5.5 μM (**1**) or 4.0 μM (**2**) at corresponding pH levels before photolysis. There seems to be no significant degradation of **1** and **2** (showing absorption due to the O → W) or Ti) charge-transfer bands around at $\lambda_{max} = 270$ and 260 nm, respectively) on changing solution pH levels, as implied by little change in the absorption bands. During the photolysis
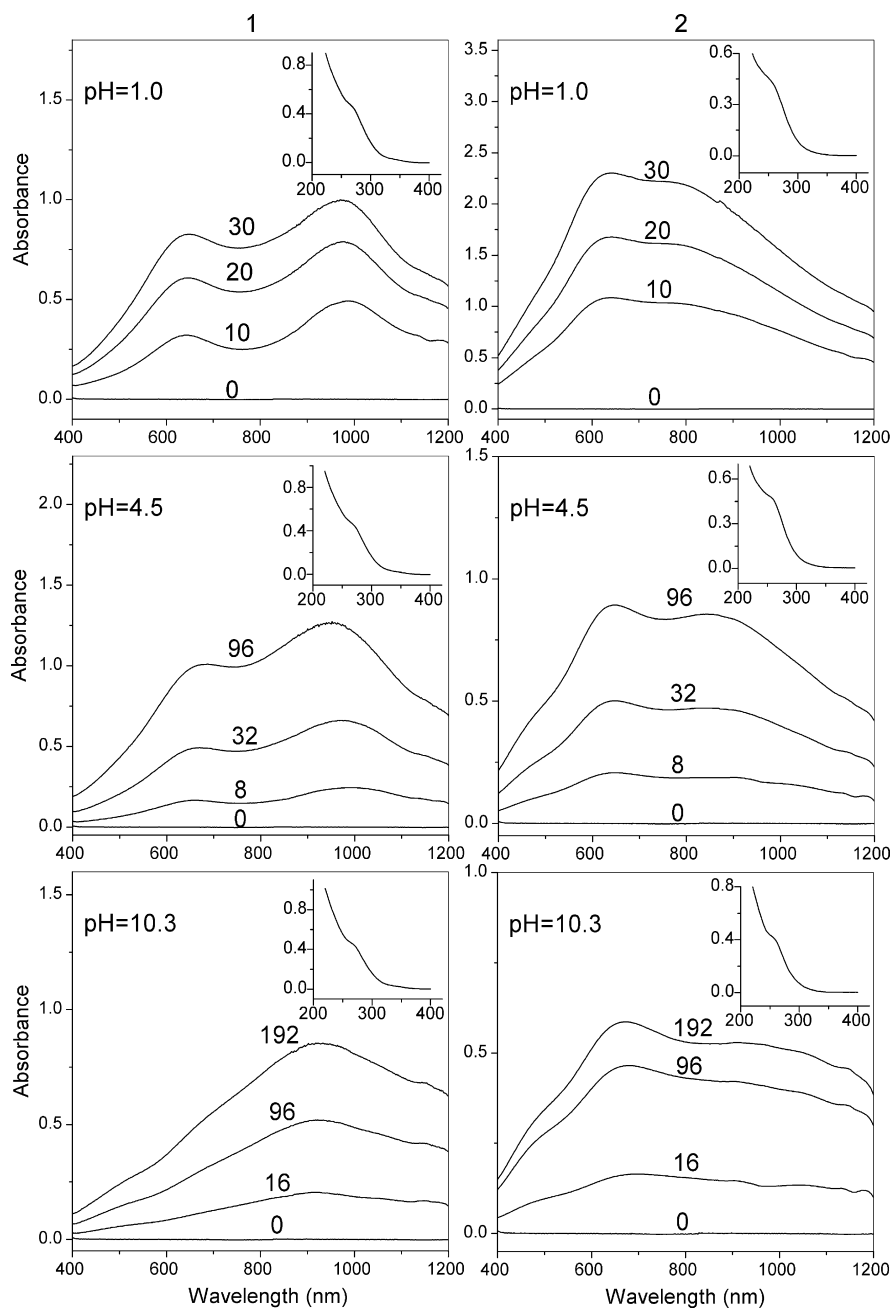
Fig. 3. Electronic absorption spectral changes during the steady-state photolysis of deaerated aqueous solutions containing 0.72 mM (**1**) and (**2**) and 2.5 M MeOH at pH levels of 1.0, 4.5, and 10.3. Inset shows the UV spectrum of the aqueous solutions containing 5.5 μM (**1**) and 4.0 μM (**2**) at corresponding pH levels before photolysis.

of **1** absorption bands around at $\lambda_{max} = 650$ and 920–990 nm are developed, and the latter is shifted to shorter wavelengths at higher pH levels. In contrast, for **2** absorption bands around $\lambda_{max} = 640$ and 800–960 nm are developed and the latter is shifted to longer wavelengths at higher pH levels. Such a pH dependence of the absorption spectra of the photolyte reflects the pH dependence of preponderance of two types of inter-valence charge-transfer bands Ti^{III}–O–$W^{VI} \leftrightarrow Ti^{IV}$–O–$W^{V}$ and W^{V}–O–$W^{VI} \leftrightarrow W^{VI}$–O–$W^{V}$ in the electronic structure of the blue species, the former is dominant in acidic media of pH ≤ 2, as discussed below.

The photoexcitation of the O → W (or Ti) charge-transfer bands for **1** or **2** in the presence of MeOH leads to the forma-tion of reduced (**1**) or (**2**), two protons (H^{+}), and HCHO under the steady-state condition. The photoreduced (**1**) or (**2**) species could be oxidized to parent species with coupling with the H_2-formation, if the oxidation potential of the reduced species were negative enough to reduce H^{+} to H_2. A more negative oxidation potential of the photoreduced species could be suggested by the first electrochemical redox-waves for **1** and **2**, as shown below. In such a case, one can expect a stoichiometric relationship among reduced (**1**) (or (**2**)), H_2, and HCHO as photoproducts. Optimal
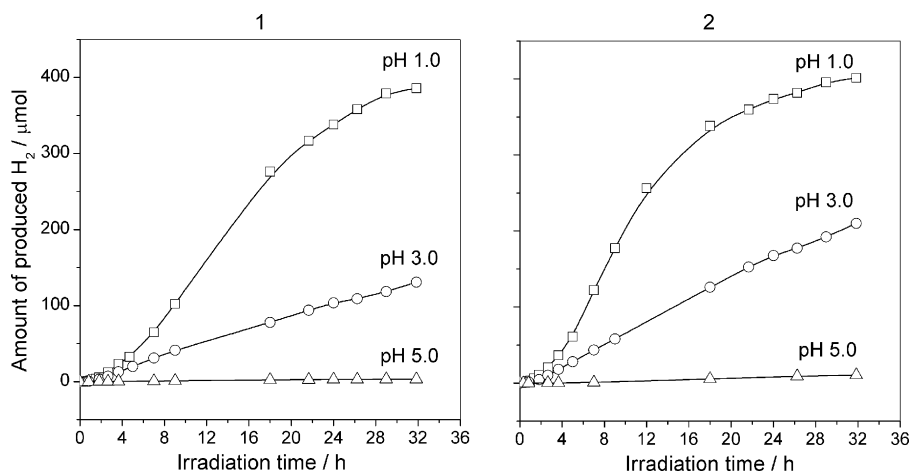
Fig. 4. Plots of amounts of H_2 produced against irradiation time on a variation of solution pHs for **1** and **2**: 0.72 mM (**1**) or (**2**) and 0.25 M MeOH under the irradiation of $\lambda > 300$ nm light.

concentrations of photocatalyst and MeOH for the photolysis were 0.7–2.0 mM and 2.0–2.5 M, respectively. Fig. 4 shows plots of amounts of H_2 produced against irradiation time on a variation of solution pHs for **1** and **2**. As shown in Fig. 4, the photolysis of **1** and **2** favorably proceeds with increasing solution acidity: quantum yield (Φ) values for H_2 and HCHO, produced at the end of the 313 nm light photolysis, for the sample solution containing 0.72 mM (**1**) or (**2**) and 2.5 M MeOH at pH 1.0 were $\Phi_{H_2} = 7.6 \times 10^{-4}$ and $\Phi_{HCHO} = 8.0 \times 10^{-4}$ for **1**, and $\Phi_{H_2} = 9.6 \times 10^{-4}$ and $\Phi_{HCHO} = 1.0 \times 10^{-3}$ for **2**. At pH 4.4 $\Phi_{H_2} = 1.7 \times 10^{-5}$ and $\Phi_{HCHO} = 2.7 \times 10^{-5}$ for **1**, and $\Phi_{H_2} = 2.1 \times 10^{-5}$ and $\Phi_{HCHO} = 3.2 \times 10^{-5}$ for **2**. The pH dependence of the photolysis may be related with both the lifetime of the excited $O \rightarrow W$ (or Ti) charge-transfer triplet states [20] and the electrochemical reversibility (as described below) of the photocatalyst for the redox reaction with MeOH. The former will increase with an increase in the protonation replacing the hydration of the excited triplet states (leading to the relaxation of excitation energy through a strong coupling with high frequency OH oscillators of hydrated water molecules) [21]. The photoreduced blue species remaining in the photolyte

can be oxidized to the colorless parent species accompanied by H_2-formation with obeying first-order kinetics on blue species concentration in the dark. Fig. 5 shows the first-order kinetics behavior (8.6×10^{-2} h^{-1} for **1** and 9.8×10^{-2} h^{-1} for **2**) for the oxidation process at 60 °C in the dark for the photolyte of the deaerated solutions containing 0.72 mM (**1**) or (**2**) and 2.5 M MeOH at pH 1.0, when the blue species is monitored by the absorption at 992 and 640 nm for **1** and **2**, respectively. The first-order rate constant for the oxidation process in the dark decreased with increasing solution pH, which will correspond to a decrease of the protonated Ti^{III} sites shown below. The first-order oxidation of the reduced species for the H_2-formation in the dark implies that the photoredox reaction of **1** and **2** with MeOH at pH 1.0 involves multi (at least two)-electron process, which would be associated with the D_{3h} Keggin-dimeric structure of **1** and **2**.

3.4. Electrochemistry

Fig. 6(a)–(c) shows a cyclic voltammogram, a d.c. polarogram of the wave around -0.43 V, and a differential pulse polaro-
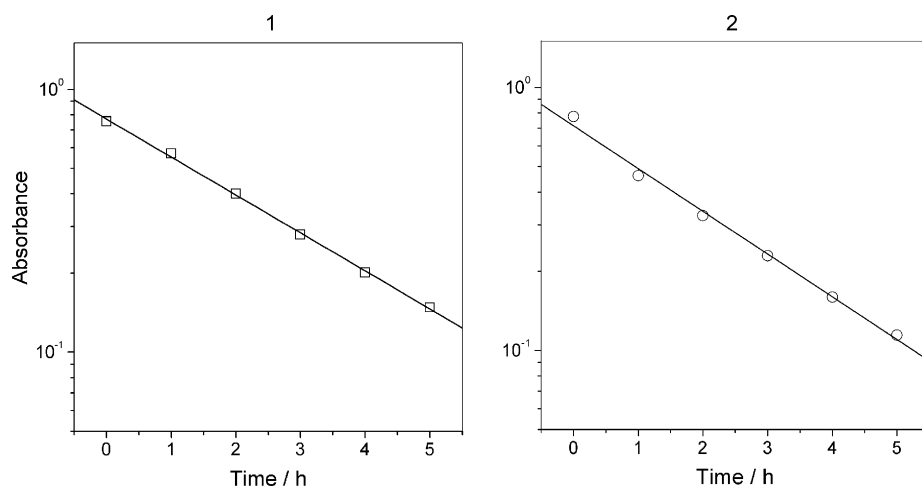

Fig. 5. First-order kinetics plot of the decoloration process at 60 °C in the dark for the photolyte of the deaerated solutions containing 0.72 mM (**1**) or (**2**) and 2.5 M MeOH at pH 1.0. The decoloration is monitored by the absorption at 992 and 640 nm for **1** and **2**, respectively. The decoloration rates are 8.6×10^{-2} for **1** and 9.8×10^{-2} h^{-1} for **2**.
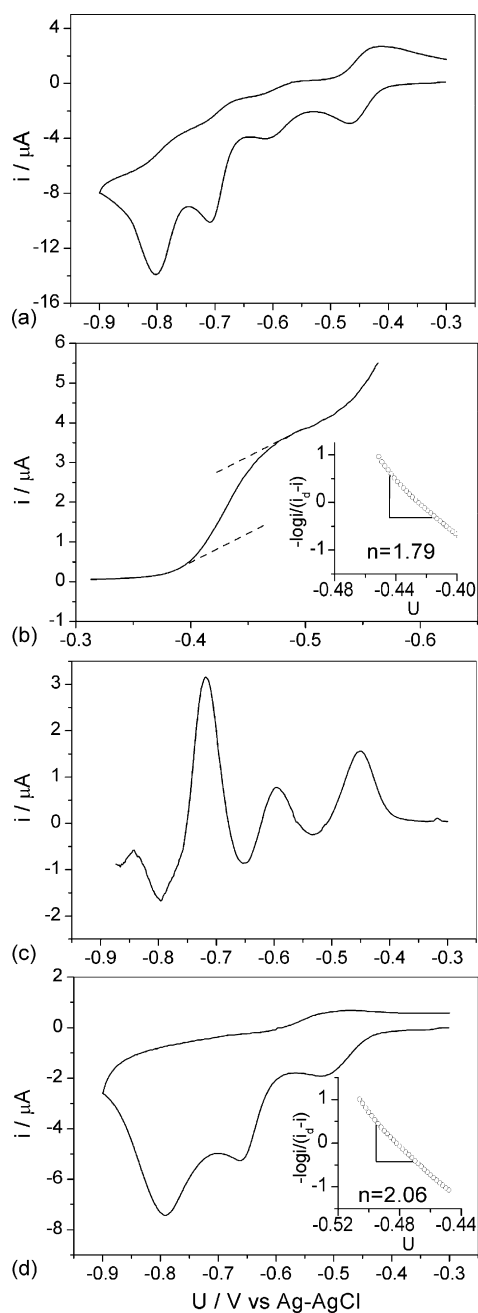
Fig. 6. Cyclic voltammogram (a), d.c. polarogram of the first redox wave around -0.43 V (b), and differential pulse polarogram (c) for **1** (1 mM) at pH 1.0 (with 0.1 M KCl). Cyclic voltammogram (d) of **2** (1 mM) at pH 1.0 is also shown for comparison. Insets in (b) and (d) indicate the polarographic analysis of the first redox wave for **1** and **2** at pH 1.0, respectively. All the cyclic voltammograms are measured at scan rate of 25 mV s^{-1}.

gram for **1** at pH levels of 1.0, respectively. Four redox waves are observed: two-electron quasi-redox wave at $E^0 = -0.43$ V (as a d.c. polarographic analysis showed the approximate reversibility of the 1.8-electron reduction–oxidation step with $E_{1/2} = -0.43$ V, in Fig. 6(b) inset) corresponds to the reduction and oxidation of the central corner-shared TiO$_6$ octahedral linkage of the molecule (step 1 in Scheme 1), the redox-wave at $E^0 = -0.54$ V corresponds to the reduction and oxidation of another corner-shared TiO$_6$ octahedral linkage (step 2 in

Scheme 1), and other two successive redox-waves around at $E^0 = -0.7$ and -0.8 V are probably attributed to multi(more than three)-electron reductions of WO$_6$-octahedra in the Keggin half-molecule. The potential difference (36 mV) between the anodic and cathodic peaks (-0.430 and -0.466 V) for the $E^0 = -0.43$ V wave also supports two-electron reduction–oxidation step. The other three waves, especially the $E^0 = -0.7$ and -0.8 V waves, exhibit a large irreversibility. The differential pulse polarogram suggests two- and four-electron reductions for $E^0 = -0.54$ and -0.7 V waves, respectively, if the $E^0 = -0.43$ V wave is two-electron step. The fact that the cyclic voltammogram of the D_{3h}-structural $[(V^{IV}O)_3(SbW_9O_{33})_2]^{12-}$ anion providing the tris(vanadyl) moiety sandwiched by two [SbW$_9$O$_{33}$]$^{9-}$ ligands showed three successive quasi-reversible redox waves (due to V$_2^{IV}$V^V/V$_3^{IV}$, V^{IV}V$_2^V$/V$_2^{IV}$V^V, and V$_3^V$/V^{IV}V$_2^V$) in aqueous solutions [22] supports that the cyclic voltammogram of D_{3h}-structural (**1a**) shows the involvement of two successive redox-waves due to the reduction and oxidation of the different corner-shared TiO$_6$ octahedral linkages in the central of anion. Fig. 6(d) shows also three successive waves (around at -0.48, -0.62, and -0.76 V) of **2** at pH 1.0 for comparison. The d.c. polarogram of the -0.48 V wave at pH 1.0 for **2** showed also two-electron quasi-redox wave at $E^0 = -0.48$ V (as shown by approximate reversibility of the 2.1-electron reduction–oxidation step with $E_{1/2} = -0.48$ V, in Fig. 6(d) inset). Slightly high negative potentials (50 and 80 mV) for the first and second reduction–oxidation waves for **2** at pH 1.0 in comparison with **1** may arise from slightly stronger bondings of both the W$_{belt}$–O–W$_{cap}$ and the two-half connecting Ti–O–Ti linkages for **2**, as suggested by slightly larger bond-angles (Appendix B). An increase in the solution pH levels up to around 7 brought about negative shift of the potential for all the redox waves with an increase of the irreversibility: for example, cyclic voltammograms of **1** and **2** at pH 4.9 showed four waves (around at -0.77, -0.90, -1.08, and -1.15 V) and three waves (around at -0.85, -0.94, and -1.2 V), respectively. The increase in the irreversibility of the first two-electron redox wave with increasing solution pH for **1** and **2** seems to be related with the decease in the photolysis with increasing solution pH levels (Fig. 4).

3.5. ESR spectra of photoreduced blue species

The photolysis of **1** or **2** in highly acidic media (at pH levels lower than 2) results in an observation of the Ti^{III} site, instead of the W^V site for the case at higher pH levels (>2). Fig. 7 shows the ESR spectra of the deaerated aqueous solutions containing 0.72 mM (**1**) or (**2**) and 2.5 M MeOH at 77 K after UV irradiation. Within 1 h after the photolysis of **1** (and **2**) at pH 1.0, the localized H$^+$–interacting Ti^{III}O$_6$ octahedron sites were observed with axially symmetric g and ^{1}H-superhyperfine tensors ($g_\parallel = 1.979$, $g_\perp = 1.909$, $A_\parallel \approx 2.5 \times 10^{-3}$ cm^{-1} = 74 MHz and $A_\perp \approx 4.2 \times 10^{-3}$ cm^{-1} = 125 MHz for **1** and $g_\parallel = 1.983$, $g_\perp = 1.906$, $A_\parallel \approx 2.1 \times 10^{-3}$ cm^{-1} = 62 MHz and $A_\perp \approx 4.6 \times 10^{-3}$ cm^{-1} = 138 MHz for **1**) at 77 K, as exemplified for **1** in Fig. 7(a). The localization of 3d^1-electron at each Ti site of the corner-shared TiO$_6$ octahedra is implied by small Ti–O–Ti bond-angles (131° and 135° in Table S3). Interestingly, the 1 h
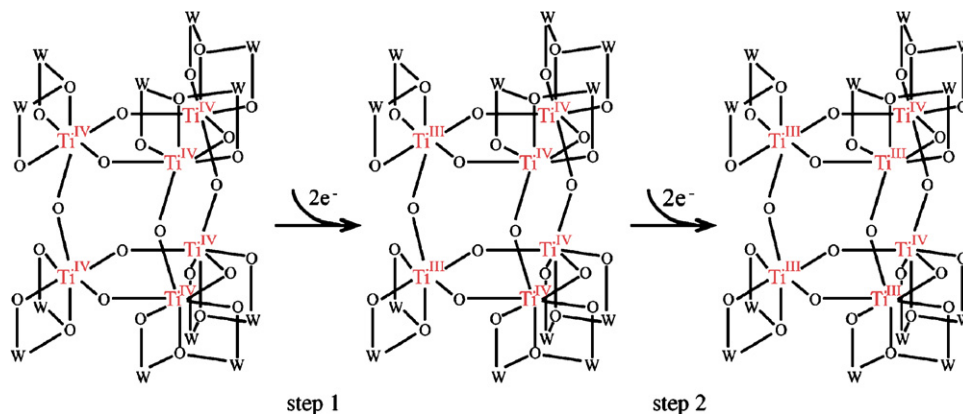
Scheme 1.

photolyte of **1** (or **2**) at pH 7.0 exhibits a different axial symmetric g tensor ($g_\parallel = 1.798$ and $g_\perp = 1.760$) with broad peak-to-peak line width of about 8.9 mT due to $W^V O_6$ octahedra at 77 K, as shown in Fig. 7(b). The ESR spectrum of the deaerated aqueous solutions containing 0.72 mM $Na_{8.5}H_{1.5}[GeW_9O_{34}]\cdot20H_2O$ (with disordering of A-α/A-β ≈ 1/9 [12]) and 2.5 M MeOH
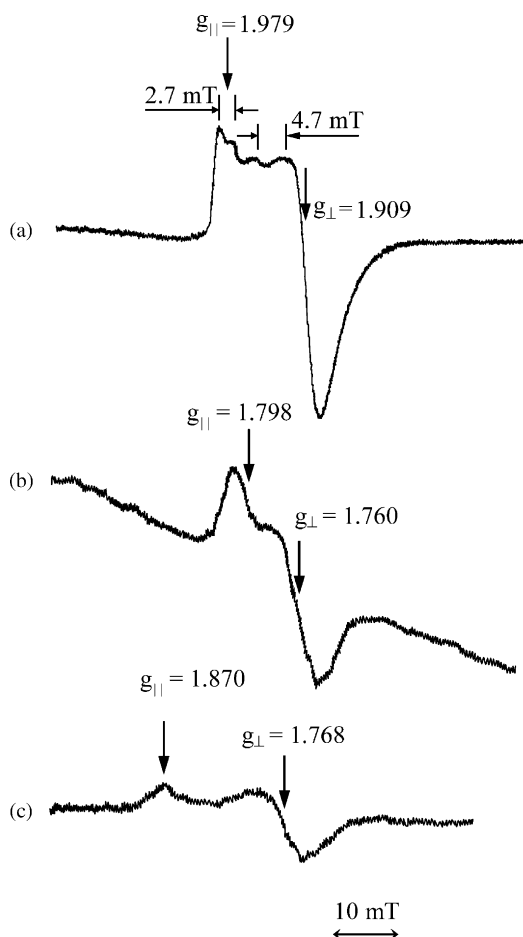

(a)

(b)

(c)

Fig. 7. ESR spectra of the deaerated aqueous solutions containing 0.72 mM (**1**) and 2.5 M MeOH at 77 K after 1 h UV irradiation at pH levels of 1.0 (a) and 7.0 (b). ESR spectrum (c) of the deaerated aqueous solutions containing 0.72 mM $Na_{8.5}H_{1.5}[GeW_9O_{34}]\cdot20H_2O$ and 2.5 M MeOH at 77 K after 1 h UV irradiation at pH 4.1 is also shown for comparison.

at 77 K after 1 h UV irradiation at pH 4.1 indicates the axial symmetric g tensor ($g_\parallel = 1.870$ and $g_\perp = 1.768$) also with broad lines of about 8.9 mT line-width due to $W^V O_6$ octahedra, as shown in Fig. 7(c). The broad line of the W^V-signal indicates the delocalization of $5d^1$-electron over the WO_6 octahedral lattice through the corner-shared W_{belt}–O–W_{cap} and W_{belt}–O–W_{belt} likages (with large W–O–W bond angles of approximately 150° and 160°, respectively, in Table S3) over the $\{GeW_9O_{34}\}$ lattice in the half molecule at 77 K, in contrast to the $3d^1$-electron localized at $Ti^{III}O_6$ octahedron site. A plausible superhyperfine interaction of the localized paramagnetic Ti^{III} $3d^1$-electron with one H atom is approximately four-fold stronger than that of the localized Mo^V $4d^1$-electron ($\approx 1 \times 10^{-3}$ cm^{-1}) [18]. Since the D_{3h}-structure of **1a** or **2a** allows equivalent single-electron reductions of two half molecules in the redox reaction between the O → W (or Ti) charge-transfer photoexcited triplet states and MeOH, it is reasonable to assume that the photolysis of **1** or **2** results in the two-electron redox reaction (to yield a Ti^{III}–O–Ti^{III} linkage) at the corner-shared TiO_6 octahedra in the center of molecule, as also supported by the occurrence of two-electron reduction–oxidation wave for the first electrochemical redox process (Fig. 5). As shown in Fig. 7(a) and (b), the ESR spectrum change of the photolyte on high acidification indicates an intramolecular electron transfer of the paramagnetic electron from WO_6 octahedra to the TiO_6 octahedron site in the molecule which would be favored by the protonation in the lattice anions, as revealed for the photolysis of $K_7[PTi_2W_{10}O_{40}]\cdot6H_2O$ [6]. The pH dependence of the electronic absorption spectra of the blue photolyte (Fig. 3) reflects the contribution of the two types of intervalence-charge-transfer transitions, Ti^{III}–O–W^{VI} ↔ Ti^{IV}–O–W^V and W^V–O–W^{VI} ↔ W^{VI}–O–W^V on the photoreduction of **1** or **2**, the former is dominant in strong acidic media.

4. Conclusions

The photochemical and electrochemical multi-electron reduction and oxidation processes are possible by a use of D_{3h}-symmetric Ti/W-mixed polyanions [(A-β-$GeW_9Ti_3O_{37})_2O_3]^{14-}$ (**1a**) and [(A-α-$GeW_9Ti_3O_{37})_2O_3]^{14-}$ (**2a**). The bonding between the corner-shared W_{belt}–$W_{cap}WO_6$
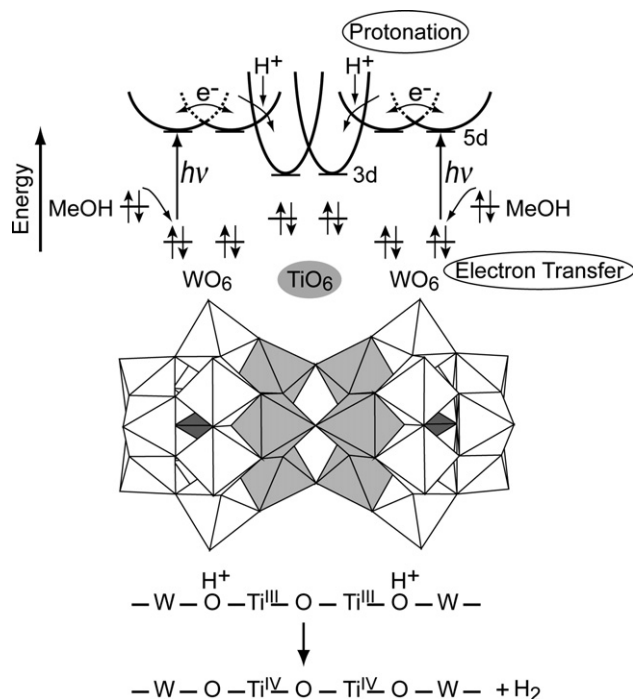
Fig. 8. An energetic scheme of two-electron H_2-generation based on the formation of Ti^{III}–O–Ti^{III} linkages arising from the intramolecular electron transfer from WO_6 to TiO_6 octahedral sites in **1** and **2**.

octahedra for **1a** is slightly weaker than for **2a**. This leads to differences in ^{183}W NMR spectral patterns and electrochemical behaviors between the two isomers. The protonation over the W_{belt} sites, favored by the replacement of partial W atoms with less positive Ti atoms, results in the symmetric intramolecular electron transfer of the injected electron from WO_6 to TiO_6 sites in two half molecules which stands for the two-electron reduction due to the formation of the Ti^{III}–O–Ti^{III} linkage at the corner-shared TiO_6 (with Ti–O–Ti bond angles $131°$ and $135°$ for **1a** and **2a**, respectively) octahedra in the center of the molecule. The highly negative oxidation potential of the two-electron (photo)reduced species of the two isomers enables the photocatalytic H_2-generation (for $MeOH \rightarrow H_2 + HCHO$) based on the multi(two)-electron reduction of two protons at the localized Ti^{III}–O–Ti^{III} sites in the anion. Fig. 8 shows an energetic scheme of the two-electron H_2-generation based on the formation of Ti^{III}–O–Ti^{III} linkages arising from the intramolecular energy transfer from WO_6 to TiO_6 octahedral sites. The double Keggin-Ti/W-mixed polyanions (**1a**) and (**2a**)

in which the three TiO_6 octahedra are linked to one another by corner-sharing in the center of the D_{3h}-molecule, provide a good model for the (photo)catalyst involving multi-electron oxidation-reduction processes.

Acknowledgements

Appendix A. Supplementary data

Supplementary data associated with this article can be found, in the online version, at doi:10.1016/j.molcata.2006.08.040.

References

[1] T. Yamase, E. Ishikawa, Y. Asai, S. Kanai, J. Mol. Catal. A 114 (1996) 237.
[2] E. Ishikawa, T. Yamase, J. Mol. Catal. A 142 (1999) 61.
[3] O.A. Kholdeeva, G.M. Maksimov, R.I. Maksimovkaya, L.A. Kovaleva, M.A. Fedotov, V.A. Grigoviev, C.L. Hill, Inorg. Chem. 39 (2000) 3828.
[4] F. Gao, T. Yamase, H. Suzuki, J. Mol. Catal. A 180 (2002) 97.
[5] M. Sugeta, T. Yamase, Denki Kagaku 57 (1989) 1190.
[6] T. Yamase, M. Sugeta, Inorg. Chim. Acta 172 (1990) 131.
[7] T. Yamase, T. Ozeki, H. Sakamoto, S. Nishiya, A. Yamamoto, Bull. Chem. Soc. Jpn. 66 (1993) 103.
[8] Y. Lin, T.J.R. Weakley, B. Rapko, R.G. Finke, Inorg. Chem. 32 (1993) 5095.
[9] G.-S. Kim, H. Zeng, J.T. Rhule, I.A. Weinstock, C.L. Hill, Chem. Commun. (1999) 1651.
[10] K. Nomiya, M. Takahashi, K. Ohsawa, J.A. Widegren, J. Chem. Soc. Dalton Trans. (2001) 2872.
[11] L.P. Kazansky, T. Yamase, J. Phys. Chem. A 108 (2004) 6437.
[12] X. Cao, H. Naruke, T. Yamase, Acta Crystallogr. E59 (2003) i116.
[13] N. Yakugakaukai, Eiseishikenhoh Chukai, Kanehara, Tokyo, 1973, p. 1065.
[14] K. Wassermann, R. Palm, H.-J. Lunk, J. Fuchs, N. Steinfeld, R. Stösser, Inorg. Chem. 34 (1995) 5029.
[15] T. Ozeki, T. Yamase, Acta Crystallogr. C47 (1991) 693.
[16] T. Yamase, T. Ozeki, S. Motomura, Bull. Chem. Soc. Jpn. 65 (1992) 1453.
[17] Unpublished Result in Preparation of Manuscript.
[18] T. Yamase, Chem. Rev. 98 (1998) 307.
[19] C.-S. Kim, H. Zeng, W.A. Neiwert, J.J. Cowan, D. VanDerveer, C.L. Hill, I.A. Weinstock, Inorg. Chem. 42 (2003) 5537.
[20] T. Yamase, K. Ohtaka, J. Chem. Soc. Dalton Trans. (1994) 2599.
[21] T. Yamase, M. Sugeta, J. Chem. Soc. Dalton Trans. (1993) 759.
[22] T. Yamase, B. Botar, E. Ishikawa, K. Fukaya, Chem. Lett. (2001) 56.